Ab initio simulation of photoemission spectroscopy in solids: Plane-wave pseudopotential approach with applications to normal-emission spectra of Cu(001) and Cu(111)

Nataša Stojić,[1,2] Andrea Dal Corso,[1,2] Bo Zhou,[3] and Stefano Baroni[1,2]

[1]*Scuola Internazionale Superiore di Studi Avanzati (SISSA), via Beirut 2-4, I-34014 Trieste, Italy*
[2]*Theory @ Elettra group, INFM-CNR Democritos, I-34012 Trieste, Italy*
[3]*TASC National Laboratory, INFM-CNR, SS 14, km 163.5, I-34012 Trieste, Italy*

We develop a method for simulating photoemission spectra from bulk crystals in the ultraviolet energy range within a three-step model. Our method explicitly accounts for transmission and matrix-element effects, as calculated from state-of-the-art plane-wave pseudopotential techniques within the density-functional theory. Transmission effects, in particular, are included by extending to the present problem a technique previously employed with success to deal with ballistic conductance in metal nanowires. The spectra calculated for normal emission in Cu(001) and Cu(111) are in fair agreement with previous theoretical results and with experiments, including a recently determined experimental spectrum. The residual discrepancies between our results and the latter are mainly due to the well-known deficiencies of the density-functional theory in accounting for correlation effects in quasiparticle spectra. A significant improvement is obtained by the LDA+U method. Further improvements are obtained by including surface-optics corrections, as described by Snell's law and Fresnel's equations.

PACS number(s): 79.60.Bm, 71.15.Ap, 71.15.Mb

I. INTRODUCTION

Photoemission spectroscopy (PES) is one of the most basic techniques for investigating the electronic properties of solids.[1,2] In practice, however, it is difficult to directly extract information from the observed spectra and theoretical considerations are necessary for precise determination of the underlying transitions. The modeling of photoemission, as well as the type and accuracy of the information that can be gained from experiments, depends on the energy range of the incident light. In the energy range of ultraviolet photoemission spectroscopy (UPS) (between 5 and 100 eV), the spectra are dominated by wave-vector-conserving transitions (direct transitions) with transition matrix elements significantly differing for any pair of initial and final states. Hence, in UPS, final-state effects play a major role. In empirical approaches, these final states are often modeled by free-electron bands, but in reality, they are influenced by the crystal potential, especially at low photon energies, and therefore, their proper description requires detailed calculations.

Early photoemission calculations, ranging from one-electron approaches to many-body formulations,[3–7] covered various aspects of the photoemission process. One-electron photoemission calculations started with the so-called three-step model,[8] which breaks the photoemission process into three independent steps: excitation of the photoelectron, its transport through the crystal up to the surface, and its escape into the vacuum. Inclusion of quasiparticle lifetimes through adjustable parameters, within the multiple-scattering Green's function formalism, led to the development of the one-step model.[9] Its modern versions can model surfaces by a realistic barrier[10] and have the potential to replace the previously adopted muffin-tin potentials by space-filling potential cells of arbitrary shape,[11] also taking into account relativistic effects.[12]

Ab initio methods based on the density-functional theory (DFT) are today considerably developed.[13,14] In particular, the plane-wave (PW) pseudopotential (PP) formulation is being applied to a wide range of properties and systems. Relativistic effects can be included in the PP both at the scalar relativistic or at the fully relativistic level, thus accounting for spin-orbit coupling.[15] This methodology, in principle, contains many of the ingredients necessary to predict a photoemission spectrum from first principles, from which information on various physical properties of the system can then be extracted. In the case of x-ray photoemission, for instance, the observed spectra are routinely compared to the density of electronic states. Considerable complications, however, arise in the *ab initio* simulation of UPS spectra, as well as in their interpretation, so that the application of state of-the-art DFT PW-PP techniques to this problem has hardly been attempted so far. First and foremost comes the difficulty of accounting for the nonperiodic nature of the electronic states involved in the photoemission process. One of the few attempts to compute photoemission spectra by using PPs was made by Stampfl *et al.*,[16] who constructed the final states by a low-energy electron-diffraction (LEED) computational technique. Second, and no less important, is the well-known inability of DFT to properly account for self-energy effects on the quasiparticle states that are the main concern of PES. This failure of DFT to accurately describe quasiparticle states is the field of intense research, currently mainly addressed by using techniques from the many-body perturbation theory, such as, e.g., the GW approximation.[17–19]

In this paper, the first problem is thoroughly addressed by calculating the transmission of electrons from the crystalline medium into the vacuum by a technique that was previously successfully employed to deal with the ballistic conductance of an open quantum system within the Büttiker–Landauer approach.[20] This technique, which was originally formulated with norm-conserving PPs, has been generalized to ultrasoft

(US) PPs by Smogunov *et al.*,[21] and this generalization is used here to calculate the transmission into the vacuum of the crystalline Bloch states. In addition to transmission, a completely *ab initio* approach to PES would require the calculation of dipole matrix elements and a proper account of self-energy effects on the electron band structure, as well as of the effects of the change in the dielectric function upon crossing the surface (surface-optics effects). Dipole matrix elements are calculated completely *ab initio* by using a technique first described by Baroni and Resta in 1986.[22] The real part of the self-energy shifts to DFT bands is accounted for semiempirically by using the LDA+*U* method, while the imaginary part (lifetime effects) is simply added as an empirical parameter. Finally, surface-optics effects are accounted for by Snell's and Fresnel's equations. While these equations could, in principle, be implemented by using a dielectric function calculated *ab initio*, for simplicity, we choose to implement them by using experimental data.[23]

As an application of our approach, we calculate the bulk contributions to the normal photoemission spectra from Cu(001) and Cu(111). Copper is a prototypical system for UPS studies, for which many theoretical results, as well as accurate experimental measurements, are available. We compare our calculations to previous theoretical studies, which were performed within the one-step and three-step models, and to experimental data. Not surprisingly, the main limiting factor in our calculations appears to be the poor description of the Cu electron bands by the local-density approximation (LDA), while transmission effects are correctly accounted for, thus providing a viable way to select and to weigh among the many available final conduction states only those that couple to vacuum states.

The paper is organized as follows: in Sec. II, we describe the theoretical method used to calculate photoemission spectra, while in Sec. III, we give some numerical details. In Sec. IV, we first discuss the contributions of different terms in our expression for the photoemission intensity on one specific example; we then present our *ab initio* results for the Cu(001) surface, which were obtained at the DFT level without empirical adjustments, followed by the results for Cu(001) and Cu(111) obtained from LDA+*U* bands and accounting for surface-optics effects. Section V contains our conclusions.

II. THEORY

In a three-step model, the photoemission current is proportional to the product of the probability that an electron is excited from an initial bulk state, ψ_i, to an intermediate bulk state, ψ_n, of energies E_i and E_n and wave vector $\mathbf{k}$, $|M_{ni}(\mathbf{k})|^2$ (in this transition, the electron momentum is supposed to be conserved, in spite of surface effects that break translational symmetry), times the probability that the electron in the intermediate state is transmitted into the vacuum, $T(E_n, \mathbf{k})$, conserving the energy and the component of the momentum parallel to the surface, $\mathbf{k}_\parallel$. By summing the composite probabilities all over the possible initial and intermediate states, we obtain the current I as a function of the photoelectron kinetic energy E_{kin} and photon energy $\hbar\omega$ by using the following standard expression:[1,24,25]

$$I(E_{\mathrm{kin}}, \hbar\omega, \mathbf{k}_\parallel) \propto \sum_{ni} \int dk_\perp |M_{ni}(\mathbf{k})|^2 T(E_n, \mathbf{k})$$
$$\times \delta[E_n(\mathbf{k}) - E_i(\mathbf{k}) - \hbar\omega]\delta[E_{\mathrm{kin}} - E_n(\mathbf{k}) + \Phi],$$
(1)

where $k_\perp$ is the component of $\mathbf{k}$ perpendicular to the surface and Φ is the work function. The three-step model that we use is, of course, an approximation which, in particular, does not properly account for coherence between the excitation process occurring in the bulk and the escape of the electron occurring at the surface. This coherence may give rise to interference effects which are, therefore, neglected in our approach.

The transition matrix element in Eq. (1), M_{ni}, is calculated from the interaction operator:

$$H_{\mathrm{int}} = \frac{e}{2mc}(\mathbf{A} \cdot \mathbf{p} + \mathbf{p} \cdot \mathbf{A}),$$
(2)

where $\mathbf{A}$ is the vector potential of the electromagnetic field, $\mathbf{p}$ is the momentum operator of the electron, e and m are the electron charge and mass, c is the speed of light, and nonlinear effects have been neglected. We will consider only the $\mathbf{A} \cdot \mathbf{p}$-type interaction, while the $\nabla \mathbf{A}$ interaction, originating from the second term in Eq. (2) and giving rise to surface emission (the divergence of $\mathbf{A}$ is significant only in a very narrow region around the surface), is neglected in accord with common practice in photoemission calculations.[9] In this paper, we shall consider normal photoemission only, i.e., $\mathbf{k}_\parallel = 0$. Energy conservation is imposed by the two δ functions. In the dipole approximation, $\mathbf{A}$ can be considered spatially constant (the wavelength of the photon beam, which is 120–2500 Å in the UPS energy range, is very large compared to the atomic spacing in crystal), and therefore, the transition matrix elements are proportional to the dipole matrix element between the propagating initial and intermediate states:

$$M_{ni} = \frac{e}{mc}\mathbf{A}\langle\psi_n|\mathbf{p}|\psi_i\rangle.$$
(3)

The vector potential $\mathbf{A}$ carries information on the light polarization, which depends on the polar (θ, defined with respect to the surface normal) and azimuthal (ϕ) angles of incidence of the photon beam. In this paper, we consider linearly polarized electromagnetic radiation, with the following convention: for *p*-polarized light, $\mathbf{A}$ is contained within the plane formed by the directions of the incident light and outgoing electron, while for *s*-polarized light, $\mathbf{A}$ is perpendicular to this plane. Thus, for *s*-polarized light, $\mathbf{A}$ is parallel to the surface for normal photoemission.

In general, when an electromagnetic plane wave impinges on a metal surface, the value of the vector potential transmitted inside the metal differs from the value in the vacuum due to the departure from unity of the medium dielectric function, $\epsilon(\omega)$.[23] The transmitted vector potential $\mathbf{A}^t$ can be calculated from the incident field $\mathbf{A}^i$, as described by Fresnel's equations, which were derived by using the Maxwell's theory and Snell's law.[26] Actually, the difference between $\mathbf{A}^t$

and $\mathbf{A}^i$ can be very large, especially for small photon energies ($\hbar\omega < 20$ eV) and large θ, as extensively discussed in literature.[24,27–31]

In order to calculate the transmission factor, $T(E_n, \mathbf{k})$, we take into account that the final state of the photoemission process is a time-reversed LEED (TRL) state, which sufficiently far from the surface is free-electron-like in the vacuum (*outer region*), while inside the crystal (*inner region*), it is a linear combination of the Bloch states available at the intermediate energy E_n. The TRL state can thus be obtained by solving the one-electron Kohn–Sham (KS) Schrödinger equation, which is subject to the appropriate boundary condition in the outer region. This task is accomplished by matching the wave functions in the inner and outer regions, using a method proposed by Choi and Ihm,[20] which was originally devised to cope with ballistic conductance and later generalized to account for US PPs.[21] In the outer region, the TRL state is a plane wave whose wave vector has a component perpendicular to the surface equal to $k_\perp = \sqrt{2mE_{\mathrm{kin}}/\hbar^2 - \mathbf{k}_\parallel^2}$. For given values of the photoelectron kinetic energy E_{kin} and parallel momentum $\mathbf{k}_\parallel$ in the inner region, the TRL state reads

$$\phi^{TRL}_{E_{\mathrm{kin}}, \mathbf{k}_\parallel}(\mathbf{r}) = \sum_m \psi_n(\mathbf{r}, \mathbf{k}_{m\perp}) t(E_n, \mathbf{k}_\parallel, \mathbf{k}_{m\perp}), \qquad (4)$$

where the sum is over all the Bloch states available at the intermediate energy, $E_n = E_{\mathrm{kin}} + \Phi$. In the intermediate region, the TRL depends on the details of the self-consistent potential at the surface, and this dependence determines the relative amplitude of the wave functions in the outer and inner regions, hence the transmission coefficient. In practice, the solution of the KS Schrödinger equation by the method of Choi and Ihm[20] provides the coefficients of the expansion of the final photoemission state in Bloch waves. These coefficients, which usually yield the total transmission, and hence the ballistic conductance, can be used to separately calculate the transmission probability into vacuum, $T(E_n, \mathbf{k}) = |t(E_n, \mathbf{k})|^2$, for each conduction band. We note that in this approach, the scattering state is normalized in such a way that both the incident plane wave and the Bloch states carry unit current.

We now discuss the way in which the two delta functions appearing in Eq. (1) can be treated in practice. The first delta function imposes energy conservation in the excitation step of the photoemission process, while the second one relates the kinetic energy measured outside the crystal to the intermediate state energy, accounting for the work function. The first delta function is usually represented as a Lorentzian:

$$\delta[E_n(\mathbf{k}) - E_i(\mathbf{k}) - \hbar\omega] = \frac{\Gamma_h/2\pi}{[E_n(\mathbf{k}) - E_i(\mathbf{k}) - \hbar\omega]^2 + \Gamma_h^2}, \quad (5)$$

which corresponds to the spectral function of the hole left behind by the excitation process[32] and results in the broadening of the initial state. The width of the distribution, Γ_h, gives the inverse lifetime of the hole and is equal to the absolute value of the imaginary part of the hole self-energy. As in the majority of other photoemission studies, we take Γ_h as an adjustable parameter. The second delta function should

be replaced by the analyzer resolution function, most commonly expressed in the form of a Gaussian:

$$\delta[E_{\mathrm{kin}} - E_n(\mathbf{k}) + \Phi]$$
$$= \frac{1}{\sqrt{2\pi}\Gamma_{det}} \exp\left[-\frac{1}{2}\frac{[E_{\mathrm{kin}} - E_n(\mathbf{k}) + \Phi]^2}{\Gamma_{det}^2}\right]. \qquad (6)$$

Γ_{det} is determined by the detector resolution and is related to the experimental energy broadening.[32]

We conclude by noticing that the bulk-emission model of photoemission neglects electron damping caused by the presence of a surface. It is implicitly assumed in Eq. (1) that $k_\perp$ conservation is perfect and the delta function for this conservation law is omitted. The $k_\perp$ conservation, $\delta(k_{n\perp} - k_{i\perp} - G_\perp)$, is usually represented by a Lorentzian, whose broadening parameter describes damping.[32] The consideration of only bulk emission is a good approximation if the damping is small, i.e., if its inverse, which is the electron escape length l_e, is long enough, at least a few lattice spacings. The escape length can be estimated from the relationship $1/l_e = \Gamma_n \delta k_\perp / \delta E_n$,[33] where Γ_n stands for the inverse lifetime of the intermediate state and $\delta k_\perp / \delta E_n$ is the inverse group velocity of the intermediate state. The escape length depends on the band structure through the $\delta k_\perp / \delta E_n$ term and on the photon energy through the empirical dependence of Γ_n on the intermediate-state energy. Empirically, one can use the relationship $\Gamma_n = 0.065 E_n$.[32]

III. NUMERICAL DETAILS

All the ingredients necessary to apply the theory outlined in Sec. II are calculated by using DFT within the PW-PP approach, as implemented in the PWscf code of the Quantum ESPRESSO distribution.[34] In particular, the calculation of transmission coefficients has been performed from the output of the PWcond component contained therein. For the exchange and correlation energy, we use the LDA with the Perdew–Zunger parametrization.[35] The interaction of the valence electrons with the nuclei and core electrons is described by a Vanderbilt US PP.[36] The use of the PP method for simulating PES deserves some comments and requires care. Modern PPs are usually designed to very faithfully reproduce the electronic structure (orbital energies and one-electron wave functions outside the atomic core region) of occupied states. Standard arguments based on the *transferability* concept ensure that the quality of the electronic structure predicted by PPs is as good in the energy range immediately above the Fermi energy (E_F), i.e., in an energy range that extends up to, say, 10–15 eV above E_F. In the present case, however, particular care has to be taken in describing the intermediate state of the transitions because these lie at a higher energy than the transferability range of currently available PPs. For this reason, we have decided to generate a highly accurate US PP, especially designed for the purposes of the present work. We used the $3d^{10}4s^14p^0$ atomic configuration of Cu, with the core radii of $r_s = 2.1$, $r_p = 2.4$, and $r_d = 2.0$ a.u. and two projectors in each of the s, p, and d channels, one of which was chosen to the energy of a corresponding atomic state at a somewhat higher energy than usually done.[37] The

PP energy bands thus obtained agree within 0.05–0.20 eV with those calculated from a highly accurate all-electron method, using the WIEN2K code,[38] up to 40 eV above E_F. Ordinary Cu PPs, generated without high-energy projectors, tend to miss some unoccupied electron bands and have larger deviations from the all-electron results with increasing energy.

To calculate $T(E_n, \mathbf{k})$, we used the self-consistent potential of a 9-layer tetragonal slab along the [001] direction separated by a vacuum space equivalent to 11 layers. We chose a vacuum space with length equal to two bulk layers as the unit cell in the left lead and two central bulklike layers of the slab as the periodic unit cell of the right lead. We used the experimental lattice constant (a=3.62 Å) without relaxing the surface layers. However, our calculation allowing relaxations along the perpendicular direction predicts −2.8% relaxation for the first layer, 0.6% for the second, and 0.2% for the third. We checked that transmission factors only negligibly change with surface relaxations in this case. Kinetic energy cutoffs of 45 and 450 Ry have been used for the expansion of the wave functions and of the charge density, respectively. These cutoffs, which are unusually large for US PPs, are a consequence of the improved transferability that we required from our custom-tailored PP. An $18 \times 18 \times 1$ Monkhorst–Pack mesh[39] was used for the slab calculation. The band structure and the matrix elements of the dipole operator were calculated from a bulk calculation in which $k_\perp$ was sampled by 860 **k** points. The matrix elements of the dipole operator have been compared to the matrix elements from the WIEN2K code, finding agreement of the order of 4% for the states of interest in this paper. For the evaluation of the second delta function from Eq. (6), we calculated the work function as the difference between the Fermi level and the electrostatic potential in the vacuum and found Φ=4.84 eV, which is in agreement with previous calculations[40] and very close to the experimental values ranging from 4.59 to 4.83 eV.[41] For Cu(111), our LDA calculations gave the value of 5.08 eV, which is in good agreement with a previous calculation [5.10 eV (Ref. [42])] and experiment [4.9 and 4.94 (Ref. [43])]. The broadening parameters which appear in Eqs. (5) and (6) are chosen as Γ_h =0.04 eV and Γ_{det}=0.07 eV.

IV. RESULTS

In this section, we first illustrate our method by discussing the various contributions to the spectrum, as calculated from Eq. (1), for Cu(001) at one specific photon frequency ($\hbar\omega$ =23 eV) and for one specific angle of incidence (θ=65°) of the incoming photon beam of p polarization. We then present calculations for a more extensive set of frequencies and incidence angles. Finally, we try to correct the two main sources of errors in our calculations by studying how the spectra are modified by the LDA+U bands and by surface optics. The corrected spectra are also presented in the case of the Cu(111) surface.

A. Illustration of the method

In Fig. 1, we show our calculated energy bands of bulk Cu. The bands are plotted in the Γ-Z direction, along [001].
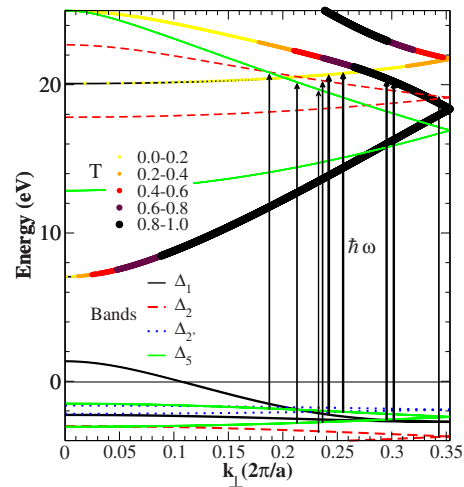

FIG. 1. (Color online) Band structure of bulk Cu along the $k_\perp$ direction for the Cu(001) surface. Among the unoccupied bands, we indicated those that have a transmission probability into vacuum larger than 0. The different point sizes and colors indicate different transmission probabilities. The zero of the energy is at the Fermi level. The direct transitions for $\hbar\omega$=23 eV are presented by arrows, while the four direct transitions which are simultaneously allowed and have nonzero transmission and dipole matrix element are shown with thick arrows.

These correspond to the bands along the Γ-X direction in the fcc Brillouin zone (BZ) refolded in the tetragonal BZ. On top of the empty bands in Fig. 1, we add information regarding $T(E_n, \mathbf{k})$ wherever it is greater than 0. This is possible because $T(E_n, \mathbf{k})$ explicitly depends on $k_\perp$ of the intermediate states.[44] Thus, reading from Fig. 1 at each intermediate energy, we can find if the propagating final states exist ($T > 0$), and if so, for which values of the intermediate $k_\perp$. In agreement with empirical intermediate-state determinations,[45] we find that a free-electron-like band properly modified by the ionic PP has the strongest coupling to the vacuum state. All the bands with nonvanishing transmission probability belong to the Δ_1 representation. This is a result of the selection rules for normal photoemission, which impose that the intermediate state be totally symmetric with respect to all the C_{4v} symmetry operations. By combining this result with the symmetry properties of the dipole matrix element, we obtain the allowed transitions for normal photoemission from the (001) surface of an fcc crystal: for the z polarization, only the $\Delta_1 \to \Delta_1$ transition is allowed, while for the x/y polarization, $\Delta_5 \to \Delta_1$ transitions are allowed.[1,46] Note, however, that some bands with Δ_1 symmetry might not be transmitted into vacuum, so symmetry alone would not be sufficient to identify the intermediate states. In the same figure, we also display nine direct transitions present in the $\hbar\omega$=23 eV case. Out of these transitions, only four satisfy selection rules and have dipole matrix elements and transmission factors that are both nonzero. Two of these transitions are of the $\Delta_1 \to \Delta_1$ type and the remaining two are of the $\Delta_5 \to \Delta_1$ type. Only one transition ($\Delta_1 \to \Delta_1$) has a large transmission factor and a large dipole matrix element, while the other of the same type has a small transmission factor. Both transitions of the $\Delta_5 \to \Delta_1$ type have a small dipole
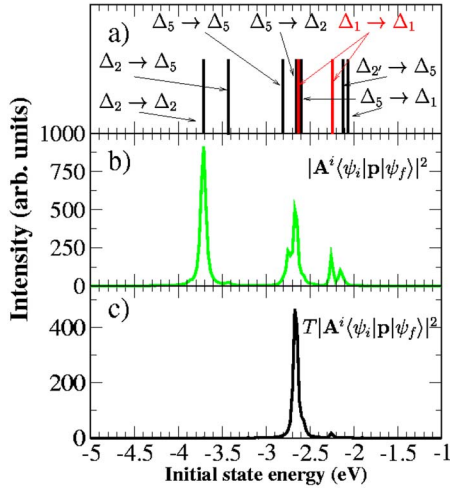
FIG. 2. (Color online) Influence of dipole matrix elements and transmission factors on the spectrum for $\hbar\omega=23$ eV and $\theta=65°$. Panel (a) presents all the allowed transitions with an indication of the symmetry of the initial and intermediate states. Panel (b) shows the effect of the dipole matrix elements. Panel (c) shows the effects of the transmission factors.

matrix element and one of them even has a small transmission factor (smaller than 0.2).

In Fig. 2, we illustrate the influence of the dipole matrix elements and of the transmission factors on the shape of the spectrum. In panel (a), we show all the direct transitions, regardless of the symmetry, their dipole matrix elements, and the transmission coefficients. In panel (b), we calculate the

photoemission spectrum setting the transmission factor to 1 for all the bands. We find that the peaks with nonzero dipole matrix elements correspond to $\Delta_2\rightarrow\Delta_2$ and $\Delta_1\rightarrow\Delta_1$ ($\Delta_2\rightarrow\Delta_5$, $\Delta_5\rightarrow\Delta_5$, $\Delta_5\rightarrow\Delta_2$, $\Delta_{2'}\rightarrow\Delta_5$, and $\Delta_5\rightarrow\Delta_1$) transitions for z polarization (x/y polarization), although the transitions with Δ_5 and Δ_2 intermediate states are not allowed for the normal emission. By including the dipole matrix elements, we obtain a spectrum in which the intensity of the peaks may change. The polarization and the direction of the incident photon beam now play an important role. For $\theta=65°$, the z-polarized transitions are enhanced with respect to transitions due to x/y-polarized light. However, neglecting the probability of the intermediate states to be transmitted to vacuum, we still have many transitions into Δ_2 and Δ_5 intermediate states which have finite intensity. Also, the relative intensities of peaks with Δ_1 intermediate states are incorrect. The introduction of the transmission factor not only selects the intermediate states with Δ_1 symmetry but also modulates the peak intensities. Thus, two peaks shown in panel (c) originate from the Δ_1 initial state, while the shoulder of the main peak on the high-energy side and almost invisible shoulder to the high-energy peak originate from the Δ_5 initial states. We note that, at variance with the rest of the paper, in Fig. 2, we used smaller broadening parameters, $\Gamma_h=\Gamma_{det}=0.015$ eV, in order to separate the different peaks.

B. *Ab initio* results

In the left panel of Fig. 3, we present our calculated spectra for five photon frequencies between 13 and 23 eV and two incident angles $\theta=18°$ and $\theta=65°$ for the p polarization.
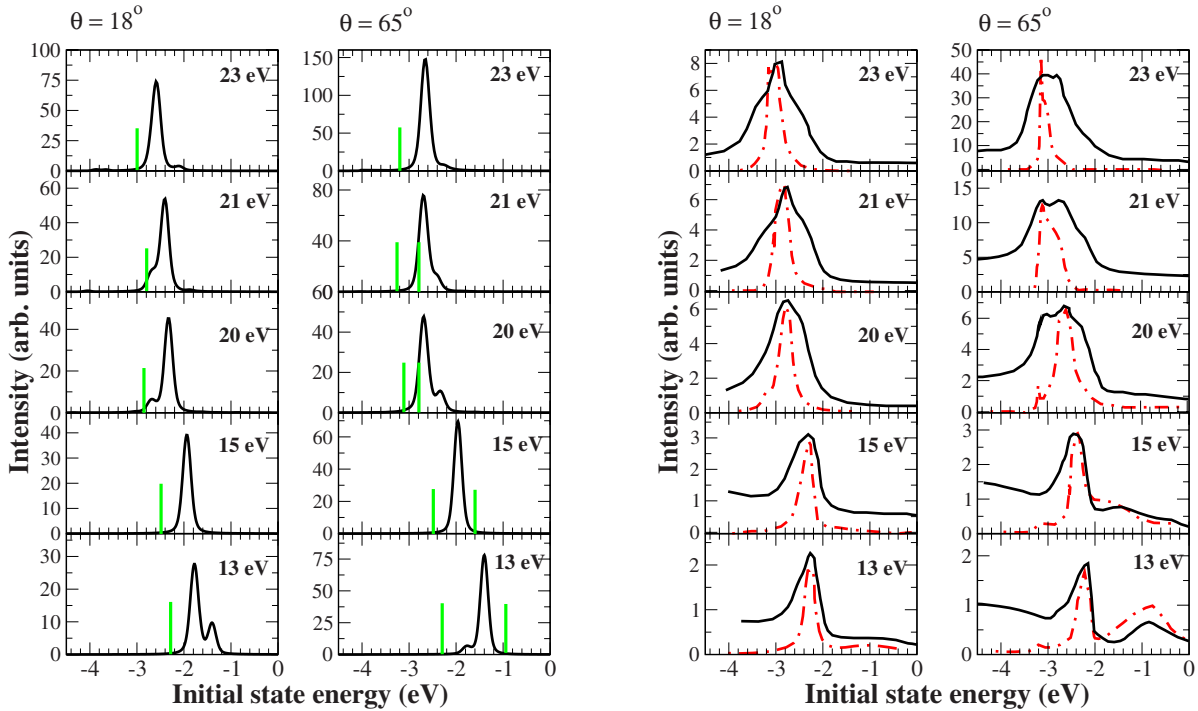

FIG. 3. (Color online) Calculated photoemission intensity for Cu(001) (left panels). The experimental spectra (dashed line), together with a previous calculation (darker full line) (Ref. 47) are shown on the right. The spectra in both panels are given for various photon frequencies and for two incident angles, $\theta=18°$ (on the left of each panel) and $\theta=65°$ (on the right). The sticks in the left panels indicate the positions of the main experimental peaks.

In the right panel, we show for comparison the experimental and previous theoretical normal-emission spectra for the same frequencies and angles.[47] Previous calculations were performed within the one-step model,[9] which were based on the nonrelativistic empirical muffin-tin potential and taking into account the surface optics through the application of Snell's law and Fresnel's equations. Our spectra in Fig. 3 do not include surface-optics effects and are calculated within the bulk photoemission model. The first approximation is quite severe and its effects will be discussed below, while the second should be sufficiently justified for this surface. Actually, for the photon energies considered here, $\delta k_\perp / \delta E_n$ is smaller than 0.05 Å^{-1} eV^{-1} and the damping (for an average photon energy of 18 eV) can be estimated to be less than 0.06 Å^{-1}. This rough estimate yields the electron escape length of about ten lattice spacings in the direction perpendicular to the surface. The choice of the incidence angle significantly influences the spectra: for $\theta=18°$, light is mostly polarized in the xy plane (the initial state belongs to the Δ_5 representation), while for $\theta=65°$, most emission is from Δ_1-like states (z polarization). Overall, our calculation reproduces the majority of the experimental peaks, albeit with a shift of about 0.2–0.6 eV toward higher energies and somewhat altered relative intensities. It is well known that the LDA, as well as the generalized gradient approximation (GGA), fails to accurately describe quasiparticle energy bands as measured by PES, and therefore, the incorrect position of the peaks has to be attributed to the error in the calculated bands.[48] The calculation within the one-step model[47] is performed with an empirical potential, and therefore, the energy bands correspond to the experimental bands rather well. The error in the positions of the energy bands can result also in a reduction or an increase in the number of peaks. At $\theta=18°$ and $\hbar\omega=13$ eV, the theoretical spectrum shows two peaks, one at -1.76 eV and one at -1.38 eV. The former is due to a transition from the Δ_5 band, while the latter originates from the Δ_1 band. Experimentally, only a single peak is present at about -2.30 eV. The spectrum for $\hbar\omega=15$ eV shows a single peak as the experiment although at a higher energy. The spectra at $\hbar\omega=20$, 21, and 23 eV show only one main peak and a small peak, missing some of the shoulders present in the experimental spectra, a feature that our result has in common with the previous calculation. The lower-energy features in the spectra $\hbar\omega=20$ and 21 eV originate from the Δ_1 bands and the higher-energy features originate from the Δ_5 bands. In the spectrum $\hbar\omega=23$, both peaks are predominantly from the Δ_5 initial state, although there are significant contributions on the low-energy sides originating from the Δ_1 initial states. These contributions are hard to discern due to a large broadening and closeness of the peaks (~ 0.1 eV).

For $\theta=65°$, the agreement is somewhat worse. The spectrum for $\hbar\omega=13$ eV has a barely visible feature in place of the main peak of the experimental spectrum, while the Δ_1 peak is significantly overestimated and at a too low energy. As we will show below, this will be corrected in part by considering the surface optics. That type of correction is quite large for small photon energies and large incidence angles.[24] Similarly to the case $\theta=18°$, the spectrum for $\hbar\omega=15$ eV has only one peak, which actually contains two transitions (from the Δ_1 and Δ_5 initial states). Due to our imprecise energy bands, both transitions are accidentally at the same energy. The experimental spectrum for $\hbar\omega=20$ eV has two peaks of roughly equal intensity, with a broad shoulder on the high-energy side, while our spectrum reproduces just one main peak and a much lower-intensity peak at a higher energy. Our spectra for $\hbar\omega=21$ and 23 eV are underestimating or missing a high-energy feature, which is present in the experimental spectra. We note that in contrast to the $\theta=18°$ case, both peaks in the spectrum for $\hbar\omega=23$ eV originate from the Δ_1 initial states, and transitions from the Δ_5 give small contributions to the high-energy sides, as seen in Fig. 2. Finally, we note that the peak intensities can be compared only to one spectrum, i.e., the intensities for different $\hbar\omega$ cannot be compared in our calculation due to the neglect of electron damping, which is energy dependent. Consequently, it is clear that the standard *ab initio* approach needs further corrections to reproduce the fine details of the experimental spectra.

C. Empirical corrections

In this section, we try to empirically correct two of the main shortcomings of our approach by using quite simple models. It is known that inclusion of self-energy effects, at least within the GW model, would be mandatory for a realistic description of the band structure.[17] Presently, however, this is beyond our capabilities mainly because it would require a nontrivial extension of the ballistic conductance code. Hence, we choose a simpler approach, using LDA+U.[49,50] LDA+U goes beyond LDA by differently treating exchange and correlation for a chosen set of states, which in this case is the copper 3d orbitals. The selected orbitals are treated with an orbital dependent potential with associated effective on-site Coulomb interaction U_{eff}, which is a function of Coulomb and exchange interactions U and J, $U_{\text{eff}}=U$-J.[51,52] The LDA+U method is most commonly known as a cure for the inability of traditional DFT implementations to predict the insulating state of some strongly correlated materials.[49] Although the theoretical foundation of LDA+U is somewhat questionable, its range of applicability is wider, and this method has indeed been successfully applied to metallic systems where the effects of electron correlations are intermediate.[53–55] LDA+U is also being successfully employed as a predictive tool in the chemistry of transition-metal molecules.[56] Furthermore, in the specific case of bulk copper, there is evidence that an account of self-interaction effects in LDA through the LDA+SIC approach leads to an improvement in the calculated bands.[57] However, the LDA+SIC approach neglects screening effects on the self-interactions, which are instead accounted for to different degrees of accuracy in the GW and in the LDA+U methods. While GW addresses screening in a more rigorous way, LDA+U can be considered as the static limit of a kind of (admittedly, rather crude) approximation to the GW method.[49]

As Cu has an almost completely filled d shell, the main effect of the LDA+U is the shift in the electron bands, while the eigenfunctions are expected to remain quite close to the

TABLE I. Comparison of different theoretical [LDA, LDA+GW corrections (Ref. 17), LDA+U, U_1 =1.5 eV, U_2=2 eV, and U_3=2.5 eV] band energies and bandwidths for copper at high-symmetry points compared to the average over several experiments (as reported in Tables I and XIII in Ref. 45). All values are in eV.

		LDA	GW	LDA+U_1	LDA+U_2	LDA+U_3	Experiment
Positions of	$\Gamma_{1,2}$	−2.18	−2.81	−2.60	−2.75	−2.92	−2.78
d bands	X_5	−1.44	−2.04	−1.85	−2.00	−2.17	−2.01
	L_3	−1.60	−2.24	−2.00	−2.17	−2.31	−2.25
	$\Gamma_{1,2}$-$\Gamma_{2,5}$	0.83	0.60	0.83	0.83	0.83	0.81
Widths of	X_5-X_3	2.94	2.49	3.01	3.04	3.05	2.79
d bands	X_5-X_1	3.40	2.90	3.53	3.57	3.61	3.17
	L_3-L_3	1.44	1.26	1.47	1.48	1.49	1.37
	L_3-L_1	3.46	2.83	3.55	3.56	3.60	2.91
Positions of	Γ_1	−9.37	−9.24	−9.25	−9.22	−9.19	−8.60
s/p bands	L_2'	−1.00	−0.57	−0.88	−0.85	−0.83	−0.85
L gap	L_1−L_2'	4.04	4.76	4.67	4.88	5.10	4.95

LDA ones.[49] Actually, we checked that, for the values of U used here, the overlap between the LDA and the LDA+U wave functions is of the order of 0.99. Thus, we kept the same transmission and dipole matrix elements calculated with the LDA wave functions correcting only the band structure.

Table I presents some results, such as the positions of the d bands and bandwidths, which were evaluated by using different methods including DFT with LDA, self-energy corrections within the GW approximation[17] calculated on top of *ab initio* DFT results, and LDA+U for three values of U_{eff}, which were all compared to the average over several experimental values.[45] The positions of the d bands at the Γ point vary greatly for different methods. The LDA calculation finds the band too shallow by 0.6 eV, while GW reproduces the experimental value quite well. LDA+U significantly improves with respect to the LDA value and for U_{eff}=2 eV gives almost the experimental value. A similar level of precision can be seen for the positions of the d bands at the L and X points, with somewhat larger deviations of the LDA and the LDA+U from the experimental value at the L point. Again, among the three values of U_{eff}, at the L and X points, the best agreement with experiment is obtained for U_{eff}=2 eV. The width of the d band at the Γ point is, instead, quite faithfully reproduced both by the LDA and the LDA+U. For other special points given in Table I, the widths remain almost constant for different U_{eff}. We note that also the positions of s/p bands and L gap improve with the LDA+U. Overall, we conclude that the LDA+U can correct the LDA bands in a significant manner and has effects comparable to the full self-energy calculation. Also, on the basis of comparison with the experimental results, we find that U_{eff}=2 eV gives the best results and we choose to use this value in the rest of the paper.

The second main problem in the calculation of the intensities of the photoemission peaks comes from the fact that the vector potential inside the solid is different from the vector potential in the vacuum. Consequently, one should correct the intensities using Snell's law and Fresnel's equations.[24,27–31] An accurate account of this effect is quite difficult. First of all, one should use a dielectric function consistently calculated within the same *ab initio* scheme used for the calculation of the other quantities. Furthermore, the effect of the surface should be properly taken into account in the evaluation of the dielectric function. However, as this would require substantial effort, we choose just to estimate the effect by using the experimental dielectric function from Ref. 23.

We report in Fig. 4 the photoemission spectrum calculated with the LDA+U bands with U_{eff}=2 eV and including the
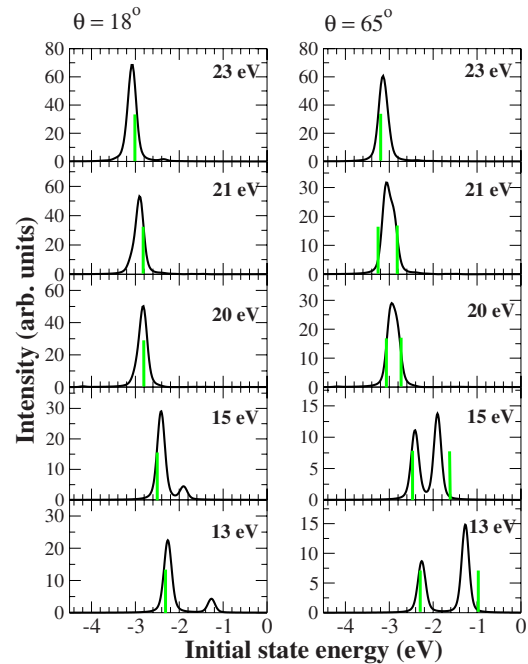

FIG. 4. (Color online) Calculated photoemission intensity for various photon frequencies for two incident angles, θ=18° and θ=65°, by using the LDA+U approach, with U_{eff}=2 eV. The sticks indicate the positions of the main peaks in the experimental spectra (and previous calculation spectra).

surface-optics corrections for the same parameters as in Fig. 3. We checked that the spectra do not show a strong dependence on the choice of U_{eff}, e.g., for $U_{eff}=1.5$ eV, the spectra are almost identical to the $U_{eff}=2$ eV case, with a small shift in energy.

In comparison with the experimental spectrum from Fig. 3, we see that the energy positions are mostly corrected. For $\theta=18°$, the spectrum for $\hbar\omega=13$ eV is improved with respect to the LDA spectrum (Fig. 3) and also in terms of the distance and relative intensities of the two peaks. For $\hbar\omega=15$ eV, the two transitions which were at the same initial energy split, giving rise to a new peak. Thus, the lower-energy peak originates from the Δ_5 band and the higher-energy one originates from the Δ_1 band. In the one-step calculation, there is only a hint of a shoulder on the high-energy side. For $\hbar\omega=20$ and 21 eV, we lose the shoulders originating from the Δ_1 initial state, which is present in the LDA spectra. This is because the bands are shifted in such a way that the transitions happen for $k_\perp$ at which the two bands are very close in energy, less than 0.2 eV difference. The spectrum for $\hbar\omega=23$ eV loses a higher-energy peak originating from the Δ_1 band, as this peak comes under the main peak from the Δ_5 band.

For $\theta=65°$, all the spectra have a significantly lower intensity with respect to the LDA as a direct consequence of surface-optics corrections. In the spectrum for $\hbar\omega=13$ eV, the positions of the peaks are improved and also the peak intensity ratio goes in the right direction as a result of the inclusion of $\epsilon(\omega)$. Nevertheless, this correction does not suffice and the intensities of the two peaks remain wrong both with respect to experiment and with respect to the one-step model. By inspecting the Cu(001) band structure in Fig. 1, we see that for $\hbar\omega=13$ eV, the two initial bands actually have different dispersions at the $k_\perp$ at which transitions are taking place (0.17 and 0.18 $2\pi/a$), whereas the dispersion of the intermediate band (the lowest unoccupied band) does not significantly change between the two $k_\perp$. The low-energy peak, which is underestimated, originates from the initial band of Δ_5 symmetry and has a smaller slope at the $k_\perp$ of the direct transition. By allowing nondirect transitions due to electron damping, this peak would get many more contributions than the peak originating from a Δ_1 band with a strong dispersion and would, thus, improve agreement with the experimental spectrum. A similar argument also holds for the spectrum for $\hbar\omega=15$ eV, which gets a new peak with respect to the LDA spectrum but whose intensity is overestimated. For $\hbar\omega=20$ and 21 eV, the high-energy peaks (of Δ_5 origin) from the LDA spectra are smeared into shoulders due to the shift of bands. For the same reason, a high-energy shoulder from the LDA spectrum for $\hbar\omega=23$ eV is lost. Overall, we conclude that the LDA+U correction is affecting all the spectra, causing the shift of all peaks, which also results in a decrease or increase in the number of peaks. The surface-optics corrections improve agreement for low photon energies and have stronger effects for $\theta=65°$. In general, both corrections improve the agreement with experiment.

Figure 5 compares our *ab initio* and corrected spectra to a recently measured experimental spectrum on the Cu(001) surface for p polarization, $\hbar\omega=17$ eV and $\theta=45°$. The experimental spectrum was measured on the Cu(001) single
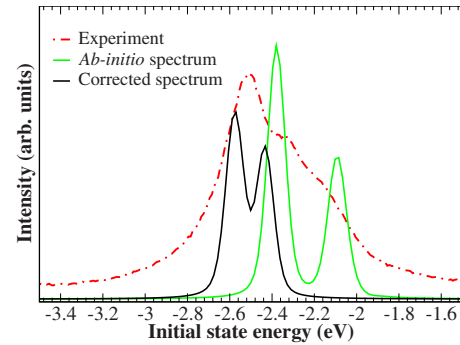

FIG. 5. (Color online) Comparison of our Cu(001) *ab initio* (light-colored full line) and corrected (dark full line) spectra with the experimental spectrum (dashed line) for $\hbar\omega=17$ eV and $\theta=45°$.

crystal surface at the APE beamline (TASC, Italy) at room temperature. It was integrated over an angular window of 1° around the normal emission. The energy resolution was estimated to be 25 meV. Both theoretical spectra have two peaks, the low-energy one originates from the Δ_1 initial band and the high-energy one originates from the Δ_5 initial band. The *ab initio* spectrum has wrong energy positions (~ 0.15 eV too high), the distance between the two peaks is too large, and the peak ratio is overestimated (1.78 instead of 1.40). The corrected spectrum shows better agreement with experiment. The positions of the peaks are closer to the experiment (~ 0.07 eV too deep), the distance between peaks is correct, while the peak ratio is somewhat underestimated (1.23). However, we cannot reproduce the high-energy broad structure present in the experimental spectrum. The experimental energy resolution and inverse lifetime of the electron hole (estimated to be $\Gamma_h=0.006E_i^2+0.01$ eV ≈ 0.04 eV)[32] cannot account for the discrepancy between theory and experiment. Also, for this photon energy, broadening due to finite electron escape length should not be pronounced. We see that not all the peaks can be explained by direct transitions only and assuming a Δ_1 intermediate state, as imposed by the selection rules for normal photoemission. We note that in Eq. (1), we disregarded the delta function describing the $\mathbf{k}_\parallel$ conservation. By performing an analysis similar to the one in Fig. 2, we have found that there are two direct transitions, forbidden by selection rules, $\Delta_5 \rightarrow \Delta_5$ and $\Delta_{2'} \rightarrow \Delta_5$, located at -2.41 and -2.38 eV in the corrected spectrum, respectively. They, also taking into account our somewhat imprecise energy positioning, might correspond to the missing peak. They have a very large dipole matrix elements and it seems likely that even a small admixing of these transitions might result in an observable structure in the photoemission intensity. The finite-acceptance angle of the electron detector means that electrons are collected from a finite part of the surface Brillouin zone (broadening of $\mathbf{k}_\parallel$). This implies that in the normal-emission spectrum, it is possible to have small contributions from the dipole-selection forbidden transitions. These issues, however, are left for future investigations.

As in the case of the (001) surface, also for the (111) surface, we present our *ab initio* calculation of the transmission factors, given on top of the empty initial bands, and plotted versus the wave vectors perpendicular to the surface
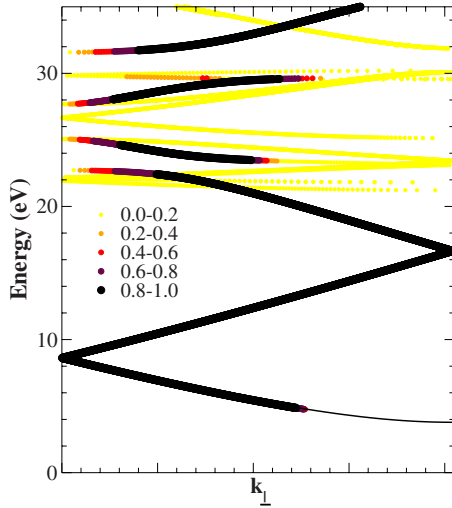
FIG. 6. (Color online) Transmission intensity plotted on top of the unoccupied electron bands along the $k_\perp$ direction for Cu(111). The symbol size and color codings for the transmission intensity are given in the legend. The Fermi level is at zero energy.

(corresponding to the Γ-L line in the fcc cell), in Fig. 6. For this surface orientation, the unit cell has three atoms and the symmetry corresponds to the C_{3v} point group. Selection rules allow only $\Lambda_1 \to \Lambda_1$ transitions for the case of z polarization and $\Lambda_3 \to \Lambda_1$ transitions for the case of x/y polarization. From Fig. 6, we conclude that for photon frequencies below 20 eV, transmission will be close to 1 for all dipole-allowed intermediate states. By using the same reasoning as for the Cu(001) case, we find that for the average photon energy of 8 eV, $k_\perp$ broadening is about 0.04 Å^{-1}. Our rough estimate yields the electron escape length of about 15 lattice spacings, which ensures that the bulk model can also be applied in this case.

In Fig. 7, we compare our calculated, experimental,[58] and previous theoretical[24] photoemission spectra from Cu(111) for various photon energies indicated on the figure. Our calculated spectra include the $\epsilon(\omega)$ and LDA+U corrections. The angle of incidence was 60° and the experiment was performed with 90% p-polarized light. The previous calculations were done within the three-step formalism,[25] using an empirical band structure generated by the combined-interpolation-scheme approach.[59] In those calculations, the authors decided to additionally suppress the A_z contributions to the spectra in order to get better agreement with the experiment. Our intensities are not adjusted beyond the corrections imposed by Snell's law and Fresnel's equations. By using the bulk-only model, we cannot reproduce the surface peak present in the experimental spectra at about −0.5 eV, which is also missing in the previous calculation.[24] However, our spectra show overall similarity to the experimental spectrum, especially considering the very general trends of changing peak positions and intensities, with increasing photon energy. In comparison with the previous calculation,[24] two spectra seem to be shifted by 0.5 eV in photon energy, i.e., our spectrum for $\hbar\omega$=7.5 eV is very similar to the one in Ref. 24 for $\hbar\omega$=7.0 eV. Furthermore, the emergence of the first bulk peak, originating from the λ_1 band at $\hbar\omega$=6.5 eV (reduced in intensity in our calculation because of an overestimation of the work function), and its shift to the deeper energies for increasing photon energy by 0.5 eV, with a larger weight on the lower states, correspond to the experimental spectra. For $\hbar\omega$=7 eV, our spectrum has one λ_1 peak, while the transition from the λ_3 band at lower energies is not seen because of the overestimated work function. Due to the poor experimental resolution, it is not easy to deduce if there are two peaks or one in the experimental spectrum. The λ_3 peak is present in our spectrum for $\hbar\omega$=7.5 eV, which reproduces well the experimental spectrum, with respect to both the peak positions and intensity. The previous calculation has a larger weight on the λ_3 peak, which is in contrast to the experiment. The single peak in our spectra for $\hbar\omega$
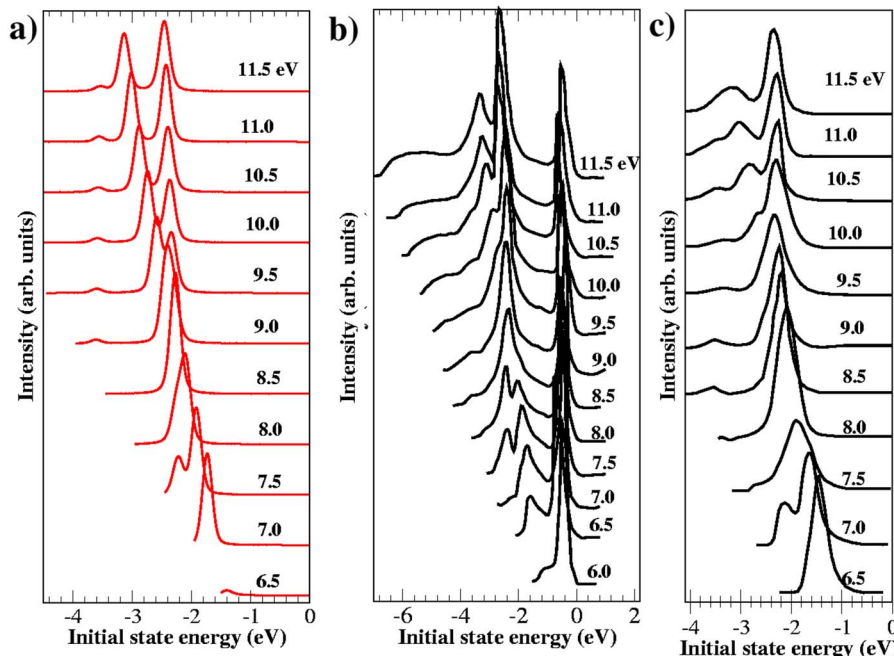

FIG. 7. (Color online) In panel (a) we present our calculated photoemission spectra from Cu(111), while the experimental spectra (Ref. 58) are in panel (b). Previous theoretical spectra (Ref. 24) are in panel (c).

$=8-9$ eV shifts weight from the right to the left shoulder (higher to lower energy) and contains contributions from both the λ_1 and λ_3 initial states (which cross at those energies). In the experimental spectrum, the same trend is present, but it starts from a lower photon energy (7.5 eV) and the spectra for lower photon energies have two peaks. For $\hbar\omega=9.0$ eV, a small peak at a lower energy emerges (~-3.1 eV), which corresponds to the λ_3 band and can also be found in all spectra for higher photon energies. It is also present in the previous calculation and in the experimental spectra, where it emerges at $\hbar\omega=8.5$ eV. Our spectra for $\hbar\omega=9.5-11.5$ eV have correct peak positions but a wrong intensity ratio of peaks, significantly overestimating the lower peak, originating from the λ_1 band, with respect to the higher-energy peak, arising from the λ_3 band. The previous calculations resolved this disagreement by artificially suppressing the *z*-polarized contributions. A likely reason for this disagreement is the neglect of surface effects in the three-step model.

V. CONCLUSIONS

In this paper, we have introduced a method for the *ab initio* low-energy photoemission calculations based on the pseudopotentials and plane waves, which has an advantage in its simplicity and unbiased basis set, with the possibility to significantly reduce the number of empirical parameters. Our method based on the bulk-emission model results in a reasonable agreement with experiment in the photon energy range up to ~25 eV. Empirical corrections, including the LDA+U and surface optics, give significant improvements. Nevertheless, in comparison with the one-step model, the intensity ratios of the photoemission peaks are still not fully reproduced. This is due to the neglect of surface damping in our model, which, in principle, could be accounted for within our approach. With respect to the experiment, some broad structures are absent in our spectra, which we interpret to originate from the forbidden transitions in the normal photoemission, caused by the detector's finite-acceptance angle and the related broadening of $\mathbf{k}_\parallel$. Further work in this direction, i.e., consideration of off-normal photoemission, is necessary to assess these effects.

[1] S. Hüfner, *Photoelectron Spectroscopy-Principles and Applications*, Springer Series in Solid State Science Vol. 82 (Springer-Verlag, Berlin, 1995).

[2] B. Feuerbacher and R. F. Wilis, J. Phys. C **9**, 169 (1976).

[3] I. Adawi, Phys. Rev. **134**, A788 (1964).

[4] G. D. Mahan, Phys. Rev. B **2**, 4334 (1970).

[5] P. J. Feibelman and D. E. Eastman, Phys. Rev. B **10**, 4932 (1974).

[6] W. L. Schaich and N. W. Ashcroft, Phys. Rev. B **3**, 2452 (1971).

[7] C. Caroli, D. Lederer-Rozenblatt, B. Roulet, and D. Saint-James, Phys. Rev. B **8**, 4552 (1973).

[8] C. N. Berglund and W. E. Spicer, Phys. Rev. **136**, A1030 (1964).

[9] J. B. Pendry, Surf. Sci. **57**, 679 (1976).

[10] M. Graß, J. Braun, and G. Borstel, J. Phys.: Condens. Matter **5**, 599 (1993).

[11] M. Graß, J. Braun, and G. Borstel, Phys. Rev. B **47**, 15487 (1993).

[12] M. Graß, J. Braun, and G. Borstel, Phys. Rev. B **50**, 14827 (1994).

[13] R. M. Martin, *Electronic Structure: Basic Theory and Practical Methods* (Cambridge University Press, Cambridge, 2004).

[14] S. Baroni, S. de Gironcoli, A. Dal Corso, and P. Giannozzi, Rev. Mod. Phys. **73**, 515 (2001).

[15] A. Dal Corso and A. M. Conte, Phys. Rev. B **71**, 115106 (2005).

[16] C. Stampfl, K. Kambe, J. D. Riley, and D. F. Lynch, J. Phys.: Condens. Matter **5**, 8211 (1993).

[17] A. Marini, G. Onida, and R. Del Sole, Phys. Rev. Lett. **88**, 016403 (2001).

[18] F. Aryasetiawan and O. Gunnarsson, Rep. Prog. Phys. **61**, 237 (1998).

[19] S. Botti, A. Schindlmayr, R. Del Sole, and L. Reining, Rep. Prog. Phys. **70**, 357 (2007).

[20] H. J. Choi and J. Ihm, Phys. Rev. B **59**, 2267 (1999).

[21] A. Smogunov, A. Dal Corso, and E. Tosatti, Phys. Rev. B **70**, 045417 (2004).

[22] S. Baroni and R. Resta, Phys. Rev. B **33**, 7017 (1986).

[23] J. H. Weaver, C. Krafka, D. W. Lynch, and E. E. Koch, *Optical Properties of Metals II* (Physics Data, Fachinformationszentrum, Karlsruhe, 1981).

[24] N. V. Smith, R. L. Benbow, and Z. Hurych, Phys. Rev. B **21**, 4331 (1980).

[25] W. D. Grobman, D. E. Eastman, and J. L. Freeouf, Phys. Rev. B **12**, 4405 (1975).

[26] M. Born and E. Wolf, *Principles of Optics* (Pergamon, Oxford, 1970).

[27] P. J. Feibelman, Surf. Sci. **46**, 558 (1974).

[28] M. A. B. Whitaker, J. Phys. C **11**, L151 (1978).

[29] A. Goldmann, A. Rodriguez, and R. Feder, Solid State Commun. **45**, 449 (1983).

[30] H. Wern and R. Courths, Surf. Sci. **152/153**, 196 (1984).

[31] H. Wern and R. Courths, Surf. Sci. **162**, 29 (1985).

[32] R. Matzdorf, Surf. Sci. Rep. **30**, 153 (1998).

[33] R. Courths, S. Hüfner, and H. Schulz, Z. Phys. B **35**, 107 (1979).

[34] S. Baroni, A. Dal Corso, S. de Gironcoli, and P. Giannozzi (URL: http://www.pwscf.org).

[35] J. P. Perdew and A. Zunger, Phys. Rev. B **23**, 5048 (1981).

[36] D. Vanderbilt, Phys. Rev. B **41**, R7892 (1990).

[37] The projector energies were -0.39 and 4.20 eV for the *s* channel, -0.05 and 2.00 eV for the *p* channel, and -0.49 and 2.80 eV for the *d* channel.

[38] P. Blaha, K. Schwarz, G. Madsen, D. Kvasnicka, and J. Luitz,

WIEN2K, An Augmented Plane Wave+Local Orbitals Program for Calculating Crystal Properties, Karlheinz Schwarz, Technical Universitat Wien, Austria, 2001.

[39] H. J. Monkhorst and J. D. Pack, Phys. Rev. B **13**, 5188 (1976).

[40] F. Favot, A. Dal Corso, and A. Baldereschi, J. Chem. Phys. **114**, 483 (2001).

[41] P. O. Gartland, Phys. Norv. **6**, 201 (1972); G. A. Haas and R. E. Thomas, J. Appl. Phys. **48**, 86 (1977); T. Fauster and W. Steinmann in *Electromagnetic waves: Recent Developments in Research*, edited by P. Halevi (North-Holland, Amsterdam, 1995).

[42] H. M. Polatoglou, M. Methfessel, and M. Scheffler, Phys. Rev. B **48**, 1877 (1993).

[43] F. R. Boer, R. Boom, W. C. M. Mattens, A. R. Miedema, and A. K. Niessen, *Cohesion in Metals* (North-Holland, Amsterdam, 1988); H. B. Shore and J. H. Rose, Phys. Rev. Lett. **66**, 2519 (1991).

[44] We note that the $T(E_n, \mathbf{k})$, had to be interpolated, so that $E_i(k_\perp)$, and $T(E_n, \mathbf{k})$, are given on the same mesh of $k_\perp$, used for integration in Eq. (1).

[45] R. Courths and S. Hüfner, Phys. Rep. **112**, 53 (1984).

[46] J. Hermanson, Solid State Commun. **22**, 7 (1977).

[47] A. Baalman, W. Braun, E. Dietz, A. Goldmann, J. Würtenberg, J. Krewer, and R. Feder, J. Phys. C **19**, 3039 (1986).

[48] V. N. Strocov *et al.*, Phys. Rev. Lett. **81**, 4943 (1998).

[49] V. I. Anisimov, F. Aryasetiawan, and A. I. Lishtenstein, J. Phys.: Condens. Matter **9**, 767 (1997).

[50] M. Cococcioni and S. de Gironcoli, Phys. Rev. B **71**, 035105 (2005).

[51] H. Sawada, Y. Morikawa, K. Terakura, and N. Hamada, Phys. Rev. B **56**, 12154 (1997).

[52] S. L. Dudarev, G. A. Botton, S. Y. Savrasov, C. J. Humphreys, and A. P. Sutton, Phys. Rev. B **57**, 1505 (1998).

[53] P. Mohn, C. Persson, P. Blaha, K. Schwarz, P. Novák, and H. Eschrig, Phys. Rev. Lett. **87**, 196401 (2001).

[54] N. Stojić and N. Binggeli, J. Magn. Magn. Mater. **320**, 100 (2008).

[55] N. Stojić, N. Binggeli, and M. Altarelli, Phys. Rev. B **73**, 100405(R) (2006).

[56] H. J. Kulik, M. Cococcioni, D. A. Scherlis, and N. Marzari, Phys. Rev. Lett. **97**, 103001 (2006).

[57] M. R. Norman, Phys. Rev. B **29**, 2956 (1984).

[58] J. A. Knapp, F. J. Himpsel, and D. E. Eastman, Phys. Rev. B **19**, 4952 (1979).

[59] E. I. Blount, in *Solid State Physics*, edited by F. Seitz and D. Turnbull (Academic, New York, 1962), Vol. 13, p. 305.